ASTM Symposium on Multiaxial Fatigue
San Diego, California
October 14-15, 1991

CONF-911048--1
DE91 018863

Propagation Behavior of Small Cracks in 304 Stainless Steel under Biaxial Low-Cycle Fatigue at Elevated Temperature*

Takashi Ogata, Akito Nitta
Central Research Institute of Electric Power Industry
Tokyo, Japan

Joseph J. Blass
Oak Ridge National Laboratory
Oak Ridge, Tennessee

---

*Prepared for the ELECTRIC POWER RESEARCH INSTITUTE/CENTRAL RESEARCH INSTITUTE OF ELECTRIC POWER INDUSTRY by the OAK RIDGE NATIONAL LABORATORY, Oak Ridge, Tennessee 37831-6285, managed by MARTIN MARIETTA ENERGY SYSTEMS, INC., for the U.S. DEPARTMENT OF ENERGY under contract DE-AC05-84OR21400.

ABSTRACT: To investigate the propagation behavior of small cracks and the relationship between crack propagation and fatigue life, strain-controlled in-phase and 90°-out-of-phase axial-torsional fatigue tests were conducted at 550°C using tubular specimens of 304 stainless steel with and without surface notches. During the tests, observations of crack initiation and propagation were frequently made using replica films and an optical microscope. Most of the fatigue life was spent in the propagation of small cracks less than 2 mm long. Regardless of loading conditions, the crack propagation rate correlated well with the equivalent shear strain range defined as a function of maximum shear strain range and normal strain range on the plane of the maximum shear strain range. The biaxial low-cycle fatigue life could be estimated from the relationship between the crack propagation rate and the equivalent shear strain range.

KEY WORDS: 304 stainless steel, biaxial low-cycle fatigue, high temperature, crack initiation, crack propagation, fatigue life prediction.

Structural components are usually subjected in service to multiaxial low-cycle fatigue in regions of stress concentration. Particularly in high-temperature power-plant components, where mechanical and thermal stresses are superimposed, loading conditions are often nonproportional. Although life predictions of components under multiaxial stress conditions are necessary for design or remaining-life assessments, an appropriate fatigue-life assessment method has not been established because limited amounts of data have been acquired due to the complexity of the test techniques and equipment.

To investigate fracture mechanisms and fatigue-life characteristics of 304 stainless steel, widely used as a structural material, under biaxial low-cycle fatigue conditions, axial-torsional fatigue tests have been conducted under proportional and nonproportional loading conditions at high temperature [1-3]. From the observation of macro crack-growth directions and fracture surfaces, fracture modes were found to be distinctly separated into either Mode I or Mode II in proportional loading, whereas mixed-mode fracture was observed in nonproportional loading. As a result, by taking the fracture mechanism into account, a new biaxial fatigue criterion was proposed based on modification of the Γ-plane of Brown and Miller [4]. In addition, surface-crack observations for a limited number of specimens during fatigue tests indicated that the initiation of small cracks had taken place at an early stage in the fatigue life [2].

Since it has also been reported that most of the low-cycle fatigue life was spent in the propagation of small cracks under uniaxial fatigue conditions [5], micro-crack propagation under biaxial low-cycle fatigue should be studied to understand the crack propagation behavior and to assess the applicability of the biaxial fatigue-life criterion. Most of the crack-propagation studies under biaxial stress fields have been conducted using cruciform specimens with through-wall center notches to investigate the effect of stress biaxiality on macro-crack propagation under Mode I loading conditions [6-8]. Small surface-crack propagation behavior has been investigated by Socie et al. using alloy 718 and 1045 steel at room temperature [9]. However, fatigue crack initiation and propagation

behaviors under proportional and nonproportional loading conditions at high temperature have not been investigated before.

In this study, crack initiation and propagation were frequently observed during biaxial low-cycle fatigue tests at high temperature using a surface-replication method. The propagation behavior of small cracks and the relationship between the rule for crack propagation rate and the criterion for fatigue-life evaluation were investigated.

Experimental Procedure

As in previous biaxial low-cycle fatigue tests [1-3], the material used in this study was 304 stainless steel, solution treated for 10 min. at 1050°C and water quenched. The chemical composition (wt%) was as follows; C:0.05, Si:0.47, Mn:0.83, P:0.03, S:0.009, Ni:9.11, and Cr:18.63. The configuration of the test specimen, a thin-wall cylinder with inside and outside diameters of 10 and 13 mm, respectively, is shown in Fig. 1. The inner surface was lapped and the outer surface was sanded with emery paper through 1000 grit, then polished lightly with alumina powder. Both smooth specimens and notched specimens were used. Each of the latter had a small hole of 0.1 mm diameter and 0.1 mm depth at mid-length, produced by electro-discharge machining after polishing.

The tests were conducted in an electro-hydraulic axial-torsional fatigue machine with high-frequency induction heating. The temperature distribution over the gage length of 12.5 mm was controlled to within ± 3°C of the test temperature. The axial and torsional strains were simultaneously and independently measured by a high-temperature biaxial strain transducer as reported previously [2].

All tests were conducted under strain control with sinusoidal strain waveforms at 550°C. Values of the strain ratio φ, defined as the ratio of torsional strain range to axial strain range, were 0, 1.7, 3.7, and ∞ for in-phase tests, in which axial and torsional strains were applied without a phase difference, and 1.7 for out-of-phase tests, in which those strains were applied with a 90° phase

difference. Thus the applied strains were proportional for in-phase tests and nonproportional for out-of-phase tests. Tests were performed at several maximum principal strain ranges for each strain ratio at a maximum principal strain rate of 10^{-3}/s. Initiation and propagation of small cracks were observed by interrupting each test at predetermined numbers of cycles. After the specimen had cooled, the outer surface of the gage length was lightly polished with diamond paste to remove the oxide layer. A 0.038-mm thick triacetate cellulose film was soaked in methyl acetate for 3-4s and applied to the entire gage length for 180s to replicate the surface. The film replica was transferred to a glass slide for examination with an optical microscope.

Results and Discussion

Observation of Surface Cracks

For smooth specimens, small cracks about 50-100μm long were observed to initiate mainly at grain boundaries approximately aligned with the direction of the maximum shear strain range, $\Delta\gamma_{max}$, for all strain ratios in in-phase tests. After initiation, the growth of small cracks undulated between the direction normal to the maximum principal strain range, $\Delta\epsilon_1$, and the $\Delta\gamma_{max}$ direction for $\varphi = 0$, while micro cracks grew in the $\Delta\gamma_{max}$ direction for $\varphi = 1.7$, 3.7 and ∞. Although cracks propagated in the $\Delta\gamma_{max}$ direction for 5 mm or more with $\varphi = 3.7$ and ∞, the direction of growth changed to the direction normal to $\Delta\epsilon_1$ at a length of 2 mm for $\varphi = 0$ and 1.7.

For notched specimens, small cracks initiated at the notch in the direction normal to $\Delta\epsilon_1$ for all strain ratios in in-phase tests and grew in the same direction as the cracks longer than 0.2 mm in smooth specimens. Linkage of small cracks was generally not observed in smooth and notched specimens tested at $\Delta\epsilon_1$ values of 1.0% or less, while linkage of small cracks occurred in some specimens tested at $\Delta\epsilon_1$ values greater than 1.0%.

Typical results of crack observations for smooth and notched specimens tested with $\varphi = 1.7$ and ∞ are shown in Fig. 2. Although there is a difference in crack-initiation direction between

smooth and notched specimens, main cracks propagated in the $\Delta\gamma_{max}$ direction in both types of specimens. On the other hand, in out-of-phase tests, micro cracks in smooth specimens initiated and grew in the circumferential direction. The growth directions of the main macro cracks observed in this study are consistent with the main crack growth directions observed in biaxial fatigue tests at 550°C reported previously [2].

Crack Propagation Behavior

Figure 3 shows the relationship between the crack length, 2l, and the cycle ratio, defined as the ratio of the cycle number, N, corresponding to a crack length of 2l, to the cycle number, $N_{l=5}$, corresponding to a crack length 2l = 10 mm, for in-phase tests of smooth specimens. Although some variation depending upon φ was observed in the 2l vs $N/N_{l=5}$ relation, small cracks about 0.1 mm long initiated as early as $N/N_{l=5}$ of about 0.2, and most of the cycles required for cracks to grow to a length of 10 mm were spent in propagation of small cracks up to about 2 mm in length. In other words, most of the low-cycle biaxial fatigue life was consumed by micro-crack propagation, as in uniaxial low-cycle fatigue [5].

It is evident from Fig. 3 that a crack length of about 2 mm was reached at $N/N_{l=5}$ of about 0.7 for $\varphi = \infty$ and $\Delta\epsilon_1$ of 1.0% or less, and the period of propagation of cracks from 2 to 10 mm in length was longer than for other values of φ. To investigate the reason for this difference, fracture surfaces of all specimens were examined with a Scanning Electron Microscope (SEM). Typical fracture surfaces at low and high magnification for $\varphi = 0$ and ∞ are shown in Fig. 4. In the fractograph for $\varphi = 0$, marks indicative of rubbing or sliding contact were observed in the region where the crack initiated and grew on the $\Delta\gamma_{max}$ plane and striations were clearly visible in the region where the crack grew in the direction normal to $\Delta\epsilon_1$. The fracture surfaces for $\varphi = 1.7$ were similar to those for $\varphi = 0$. The aspect ratio of the crack, which is the ratio of the depth to the surface half length, for both $\varphi = 0$ and 1.7, was estimated as 0.8 to 1.0 from fractographs. On the other hand, rubbing marks were observed on the entire fracture surface, as shown in the Fig. 4(b), for $\varphi = 3.7$

and ∞, where the crack grew on the $\Delta\gamma_{max}$ plane, and the aspect ratio was about 0.2-0.3. Socie et al. [9] reported aspect ratios of 0.14 in 1045 steel and 0.3-0.6 in alloy 718 with crack growth on the $\Delta\gamma_{max}$ plane under axial and torsional fatigue at room temperature. These aspect ratios are near the values obtained in this study. Thus, since the aspect ratios of main cracks that propagated on the $\Delta\gamma_{max}$ plane are smaller than those that propagated in the direction normal to $\Delta\epsilon_1$, they appear to have propagated along the surface rather than through the wall until they become relatively larger. Therefore the period of propagation of cracks from 2 to 10 mm in length was longer for $\varphi = \infty$ than for $\varphi = 0$ and 1.7, as indicated in Fig. 3. However for $\varphi = 3.7$, this tendency was not seen in Fig. 3 because applied maximum principal strain ranges were larger than 1.0% and linkage of small cracks occurred.

Figure 5 shows the relationship between crack propagation rate, dl/dn, and crack half length, l, obtained from in-phase tests with $\varphi = 1.7$ and ∞, and from out-of-phase tests with $\varphi = 1.7$. The crack propagation rate is proportional to the crack half length in the region where the crack half length is smaller than about 1 mm, i.e.

$$dl/dn \propto l \tag{1}$$

This relation holds for relatively larger crack lengths with $\varphi = \infty$. This seems to be associated with smaller aspect ratios for $\varphi = \infty$ as mentioned above.

Nishitani et al. reported that crack-propagation behavior could be studied effectively using test specimens with a small hole or partial notch [10]. Likewise in this biaxial fatigue study, crack-propagation behavior in notched specimens was very similar to that in smooth specimens for crack half lengths larger than 0.1 mm. Henceforth crack propagation behavior will be discussed without distinction between smooth and notched specimens.

In view of the influence of the maximum shear strain range, $\Delta\gamma_{max}$, on crack propagation behavior, as discussed above, the relationship for crack propagation rate should include $\Delta\gamma_{max}$ as a control parameter.

$$dl/dn = D(\Delta\gamma_{max}/2)^m l \qquad (2)$$

where D and m are material constants depending upon the strain conditions. The constants can be estimated from the relationship between dl/dn and $\Delta\gamma_{max}/2$ shown in Fig. 6. Although it is difficult to obtain precise values due to limited data, m is approximately 2.0 from Fig. 6. The crack propagation rate increases as the strain ratio decreases, or as the normal strain range $\Delta\epsilon_n$ on the $\Delta\gamma_{max}$ plane increases, for the same value of $\Delta\gamma_{max}/2$, during in-phase tests. Furthermore, significant acceleration of crack propagation rate is observed in out-of-phase tests for which $\Delta\epsilon_n$ is larger than for in-phase tests. In Fig. 7 crack propagation rate is plotted vs $(\Delta\gamma_{max}/2)^m$ l for m = 2. Although the crack propagation rate data for each strain ratio are well correlated by $(\Delta\gamma_{max}/2)^2$ l, a unified correlation of all data does not result because the crack propagation rate depends upon strain ratio, φ.

Equivalent Shear Strain Range Criterion

The influence of $\Delta\epsilon_n$ on crack propagation rate, as shown in Fig. 6, should obviously be taken into account. Both $\Delta\gamma_{max}$ and $\Delta\epsilon_n$ were already found to be controlling factors on biaxial fatigue life [1,2] based on analysis of strain range vs life results and fractographic observations, and a fatigue-life criterion or equivalent shear strain range, $\overline{\Delta\gamma}$, was proposed as a function of $\Delta\gamma_{max}$ and $\Delta\epsilon_n$, based on the modified Γ-plane. It was also reported that biaxial fatigue life under nonproportional as well as proportional loading could be well correlated with $\overline{\Delta\gamma}$. In this study, to determine the $\overline{\Delta\gamma}$ which gives the same dl/dn for any strain ratio at a given crack length, within the range where dl/dn is proportional to the crack length, iso-dl/dn contours were established on the modified Γ-plane. These

iso-dl/dn contours, obtained from the dl/dn vs $\Delta\gamma_{max}/2$ relation at a crack half length of 0.5 mm are shown in Fig. 8. Similarly shaped dl/dn contours can be obtained for crack half lengths between 0.05-1.0 mm. For in-phase tests, the iso-dl/dn contours are represented by a segment of an ellipse similar to the iso-fatigue life contours obtained in previous studies [1-3]. For out-of-phase tests with $\varphi = 1.7$ in this study, the iso-dl/dn contours are represented by straight lines, consistent with the iso-fatigue life contours obtained previously for out-of-phase tests [1-3]. The definition of $\overline{\Delta\gamma}$ for each condition is given by the following equations based on the iso-dl/dn contours.

$$\overline{\Delta\gamma} = \left[(\Delta\gamma_{max}/2)^2 + 10.5\ \Delta\epsilon_n^2\right]^{1/2} \quad \text{(In-phase)} \tag{3a}$$

$$\overline{\Delta\gamma} = \Delta\gamma_{max}/2 + 1.2\,\Delta\epsilon_n \qquad \text{(Out-of-phase)} \tag{3b}$$

The values of the material constants in these equations, given the limitation and scatter of the data, are nearly the same as the values in the fatigue-life criterion. This implies that the effect of stress-strain biaxiality on the propagation of small cracks is reflected in fatigue life as well.

The relationship between dl/dn and $\overline{\Delta\gamma}^2$l is shown in Fig. 9. dl/dn under both proportional and nonproportional loading can be correlated within a narrow band by $\overline{\Delta\gamma}^2$l, because the influence of $\Delta\epsilon_n$ on propagation of small cracks is taken into account in $\overline{\Delta\gamma}$. Therefore the crack propagation rate can be represented by following equation,

$$dl/dn = C\,\overline{\Delta\gamma}^2 l \tag{4}$$

where C is a material constant. Thus $\overline{\Delta\gamma}$ is an effective parameter to describe both fatigue life and crack propagation under biaxial fatigue loading.

The above results and discussions indicate that in the low-cycle fatigue region, where an almost linear relation exists between $\overline{\Delta\gamma}$ and fatigue life on logarithmic coordinates, fatigue life can be estimated from crack propagation rate by integrating Eq. (4) and, conversely, crack propagation rate can be estimated from the relationship between $\overline{\Delta\gamma}$ and fatigue life. Here, fatigue life was estimated from the crack propagation rate obtained in this study. The crack propagation life was estimated by integrating the upper and lower limits of the dl/dn-$\overline{\Delta\gamma}^2$l band shown in Fig. 9 from initial crack length to final crack length, assumed to be 0.1 and 2 mm respectively. Then the fatigue life band was determined by assuming that the crack propagation life occupied 80% of the fatigue life. Figure 10 shows the low-cycle biaxial fatigue-life data obtained from the previous biaxial fatigue tests and the estimated fatigue-life band of the $\overline{\Delta\gamma}$-fatigue life relation. Since most of the fatigue-life data fell within the band estimated from the crack propagation rate, the results of the estimation process are considered favorable. Since crack propagation rate and fatigue life under biaxial loading can be evaluated with $\overline{\Delta\gamma}$, it is possible to estimate these properties based on uniaxial fatigue data.

Conclusion

Crack-propagation tests of 304 stainless steel were conducted at 550°C under biaxial low-cycle fatigue conditions, including proportional and nonproportional loading. Crack initiation and propagation were frequently observed to investigate the relationship between crack propagation and the fatigue-life criterion. Results obtained in this study are summarized as follows.

1. Small cracks (about 50-100 μm in length) initiated mainly on grain boundaries approximately aligned with the direction of the maximum shear strain range under any strain ratio, φ. Crack growth undulated between the direction normal to the maximum principal strain range and the direction of the maximum shear strain range for $\varphi = 0$. Cracks grew on the plane of the maximum shear strain range for $\varphi = 1.7$, 3.7 and ∞. These observations indicate that the maximum shear strain range strongly influences crack propagation in biaxial low-cycle fatigue.

2. Most of the fatigue life was spent in propagation of small cracks less than 2 mm, where the crack propagation rate is proportional to the crack length. For $\varphi = \infty$, the linear relationship between the crack propagation rate and the crack length holds until the crack length is larger than for $\varphi = 0$ and 1.7, because cracks grew as stable surface cracks with small aspect ratios (0.2-0.4).
3. In addition to the maximum shear strain range, the normal strain range on the plane of the maximum shear strain range influences the crack propagation rate in biaxial fatigue. That is, for the same maximum shear strain range, the crack propagation rate increases as the normal strain range on the plane of the maximum shear strain range increases. The crack propagation rate under nonproportional loading is significantly accelerated due to the larger normal strain range on the plane of the maximum shear strain range for out-of-phase straining.
4. Regardless of strain conditions, the crack propagation rate could be correlated well with the equivalent shear strain range, based on the modified Γ-plane, which takes into account the effect of the normal strain range on the plane of the maximum shear strain range. Biaxial low-cycle fatigue life could be estimated from the relationship between the crack propagation rate and the equivalent shear strain range. Therefore the equivalent shear strain range is considered the most useful parameter for describing both crack propagation and fatigue life under biaxial loading.

References

[1] Kuwabara, K., Nitta, A., and Ogata, T., International Conference on Mechanical Behavior of Materials (ICM5), Vol. 2, 1987, pp. 1173-1180.

[2] Nitta, A., Ogata, T., and Kuwabara, K., Fatigue and Fracture of Engineering Materials and Structures, Vol. 12, No. 2, 1989, pp. 77-92.

[3] Ogata, T., Nitta, A., and Kuwabara, K., Proceedings, Third International Conference on Biaxial/Multiaxial Fatigue, April 3-6, 1989, Stuttgart, FRG, pp. 56.1-56.17.

[4] Brown, M. W., and Miller, K. J., Proceedings, Institution of Mechanical Engineers, Vol. 187, 1973, pp. 745-755.

[5] Nishitani, H., and Goto, M., The Behavior of Short Fatigue Cracks, K. J. Miller and E. R. de los Rios, Ed., EGF Publication 1, 1986, pp. 461-478.

[6] Hoshide, T., Tanaka, K., and Yamada, A., Fatigue of Engineering Materials and Structures, Vol. 4, 1981, pp. 355-366.

[7] Brown, M. W., and Miller, K. J., Multiaxial Fatigue, ASTM STP 853, 1985, pp. 135-152.

[8] Kitagawa, H., Yuuki, R., Tohgo, K., and Tanabe, M., Multiaxial Fatigue, ASTM STP 853, 1985, pp. 164-183.

[9] Socie, D. F., Han, C. T., and Worthem, D. W., Fatigue and Fracture of Engineering Materials and Structures, Vol. 10, No. 1, 1987, pp. 1-12.

[10] Nishitani, H., and Kawagoishi, H., Transactions, Japan Society of Mechanical Engineers, 49, 1983, pp. 431-440.

Figure Captions

Fig. 1 — Configuration of test specimen.

Fig. 2 — Crack initiation and propagation for smooth and notched specimens with $\varphi = 1.7$ and ∞; (a) smooth, $\varphi = 1.7$, (b) notched, $\varphi = 1.7$, (c) smooth, $\varphi = \infty$, (d) notched, $\varphi = \infty$.

Fig. 3 — Crack length vs cycle ratio for in-phase tests of smooth specimens.

Fig. 4 — Typical SEM fracture surfaces for given values of φ.

Fig. 5 — Crack propagation rate vs half crack length for given test conditions.

Fig. 6 — Crack propagation rate vs $\Delta\gamma_{max}/2$ for l = 0.5 mm and given test conditions.

Fig. 7 — Crack propagation rate vs $(\Delta\gamma_{max}/2)^2$l for given test conditions.

Fig. 8 — Iso-dl/dn contours on the modified Γ-plane for l = 0.5 mm and given test conditions.

Fig. 9 — Crack propagation rate vs $\overline{\Delta\gamma^2}$l for given test conditions.

Fig. 10 — Equivalent shear strain range vs fatigue life results of biaxial tests compared to prediction band based on the relationship between crack propagation rate and equivalent shear strain range.

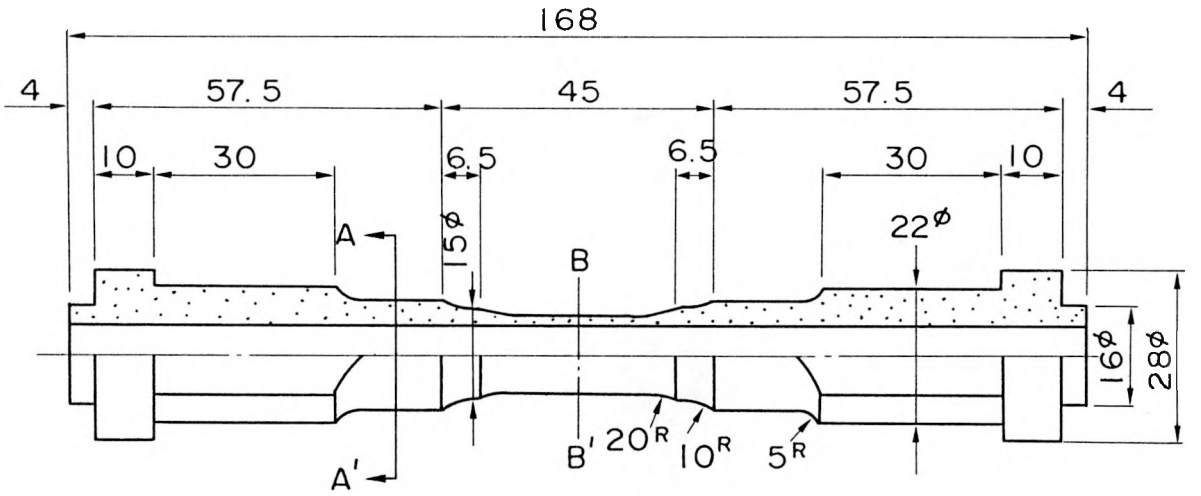

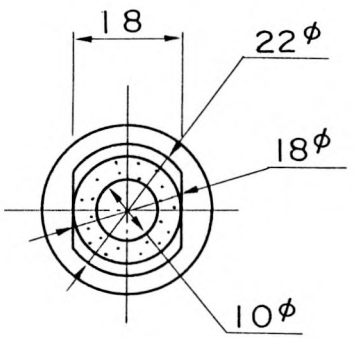

Direction A – A'

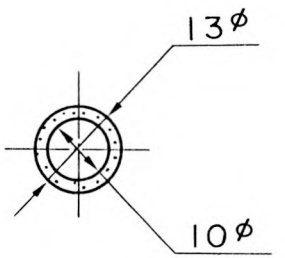

Section B – B'

Fig. 1

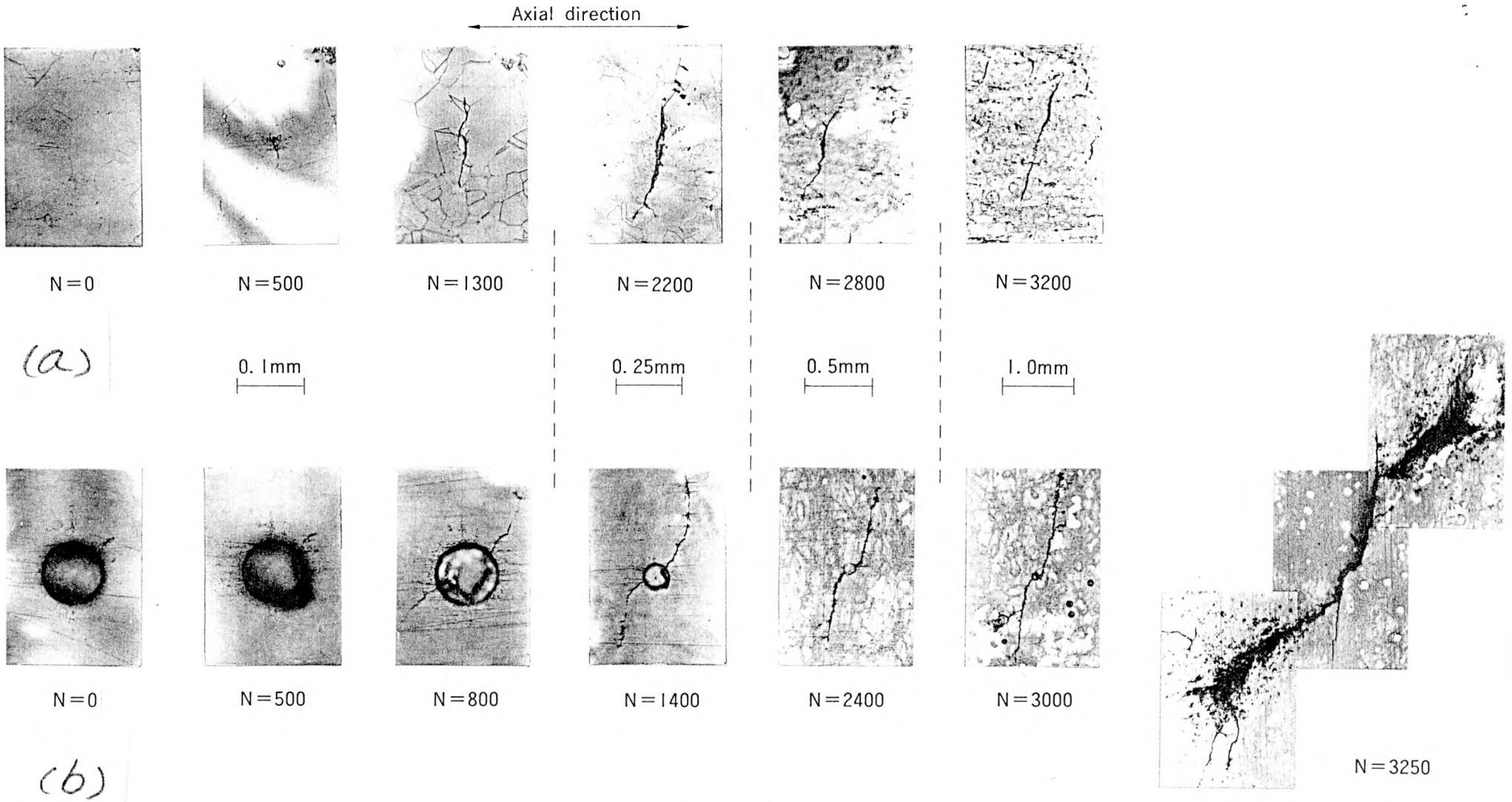
Axial direction
N=0
N=500
N=1300
N=2200
N=2800
N=3200
(a)
0.1mm
0.25mm
0.5mm
1.0mm
N=0
N=500
N=800
N=1400
N=2400
N=3000
N=3250
(b)

Fig. 2

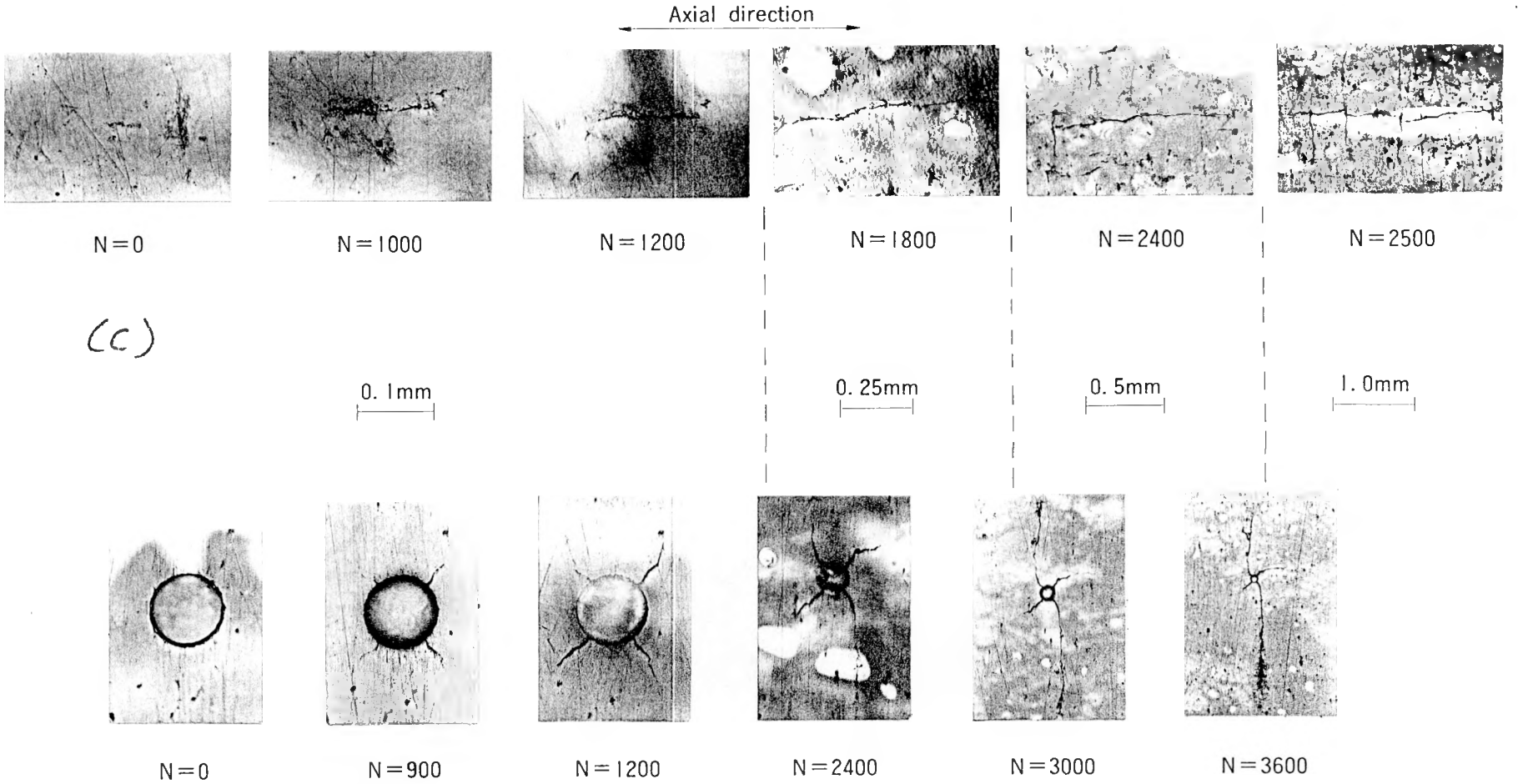
Axial direction
N=0
N=1000
N=1200
N=1800
N=2400
N=2500
0.1mm
0.25mm
0.5mm
1.0mm
N=0
N=900
N=1200
N=2400
N=3000
N=3600

(c)

(d)

Fig. 2 (Cont.)

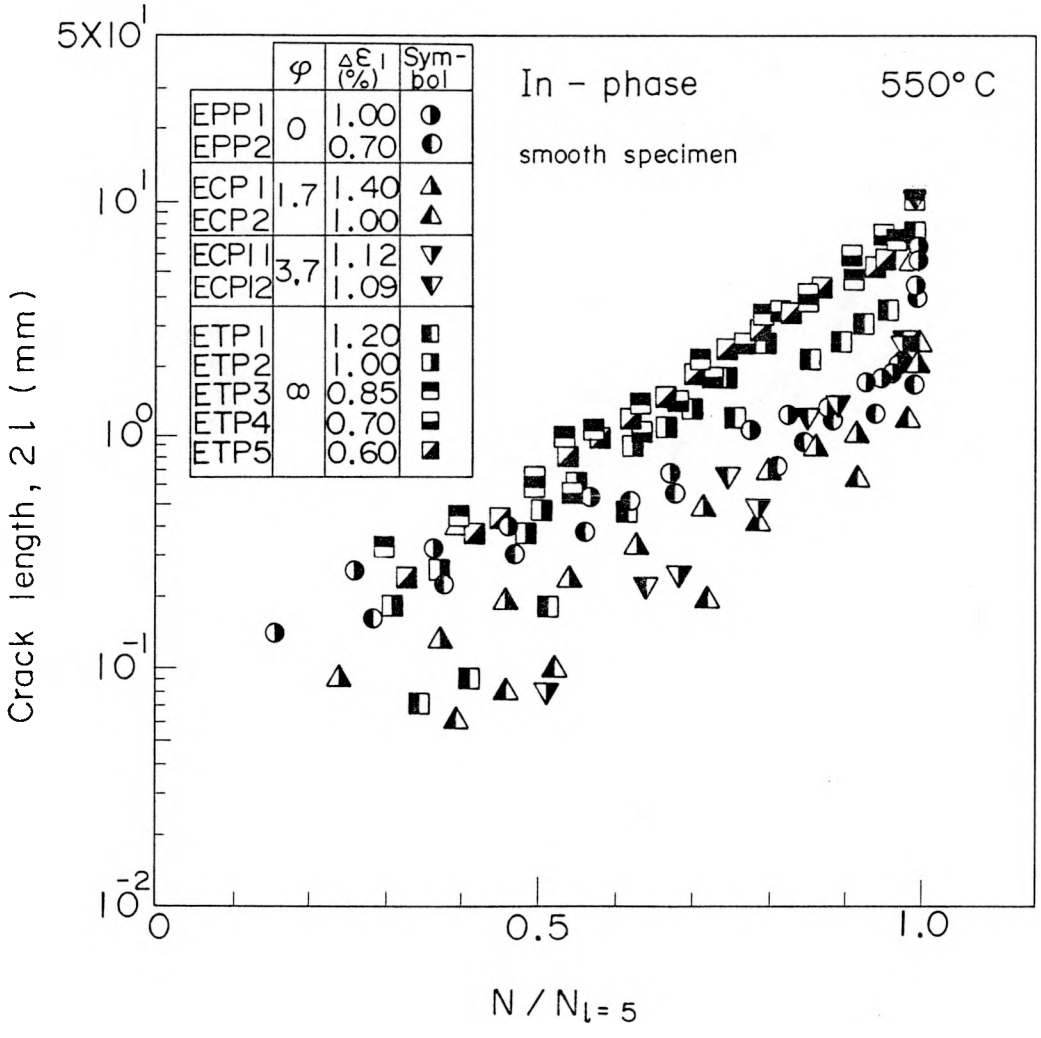
5X10^1
10^1
10^0
10^-1
10^-2
Crack length, 2l (mm)
0
0.5
1.0
N / N_l=5
In - phase
550° C
smooth specimen
φ
Δε_t (%)
Sym-bol
EPP1 0 1.00
EPP2 0.70
ECP1 1.7 1.40
ECP2 1.00
ECPI1 3.7 1.12
ECPI2 1.09
ETP1 ∞ 1.20
ETP2 1.00
ETP3 0.85
ETP4 0.70
ETP5 0.60

Fig. 3

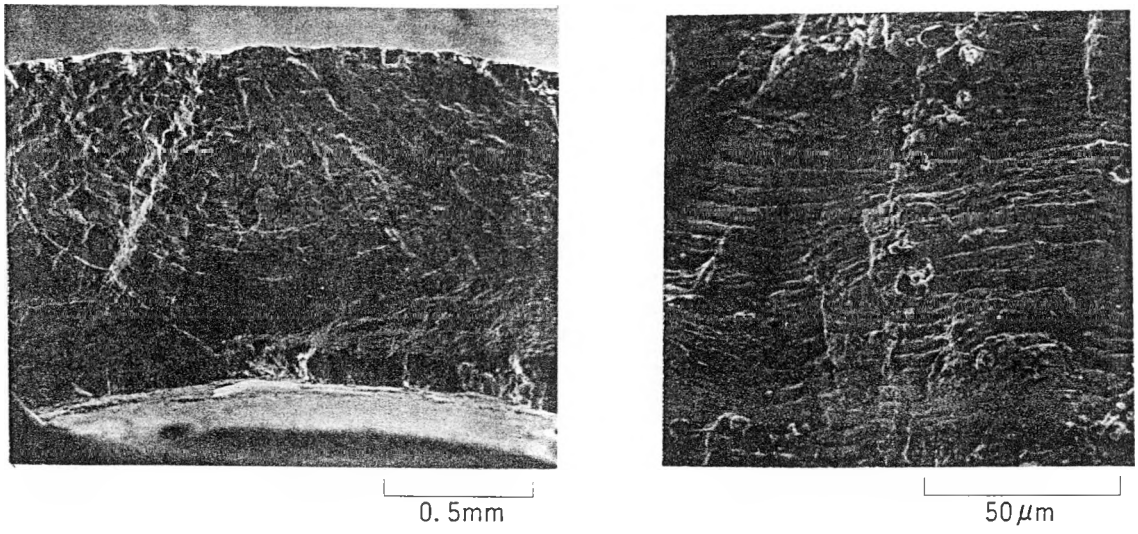

(a) $\varphi = 0$

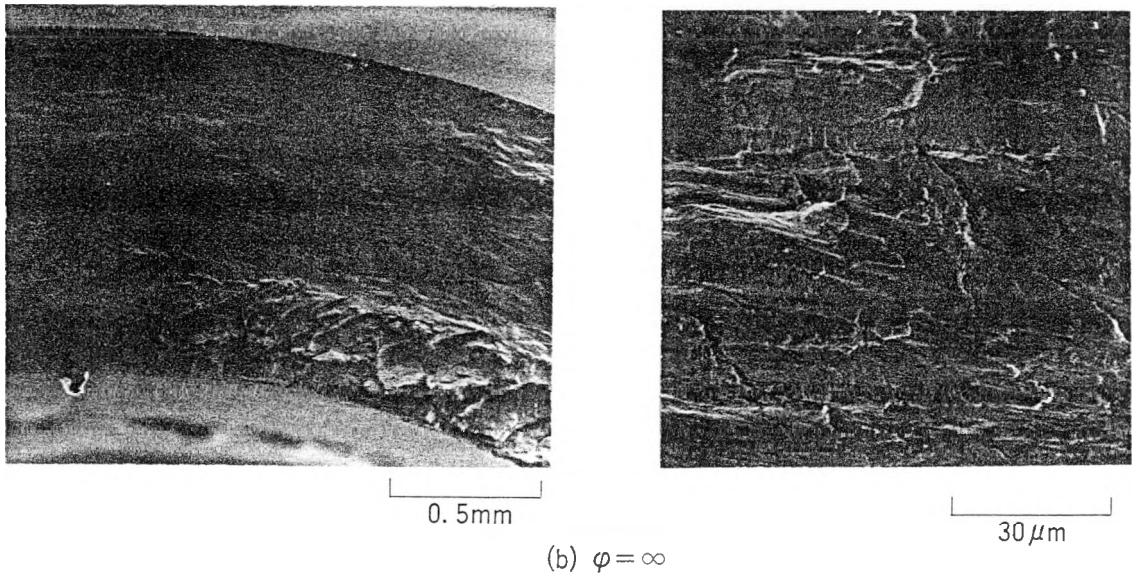

(b) $\varphi = \infty$

Fig. 4

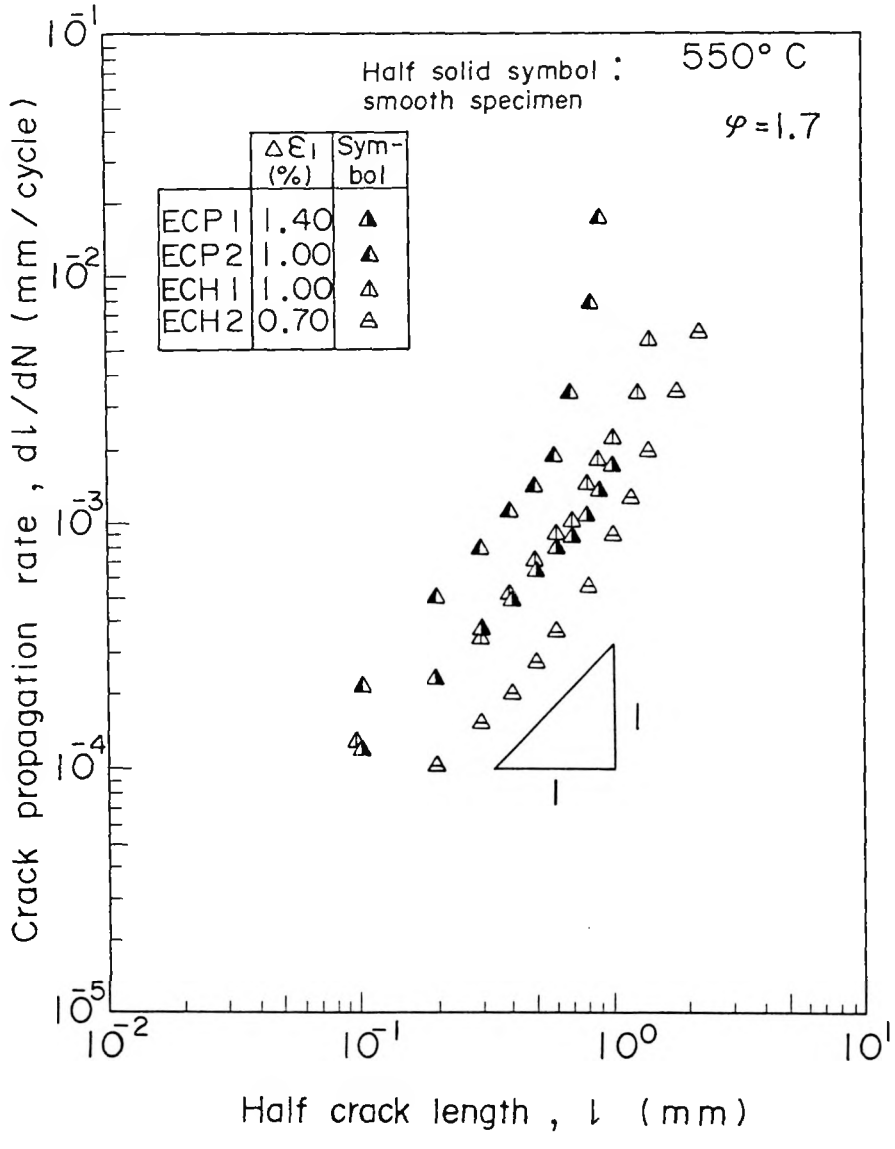

(a) φ = 1.7 (In - phase)

Fig. 5

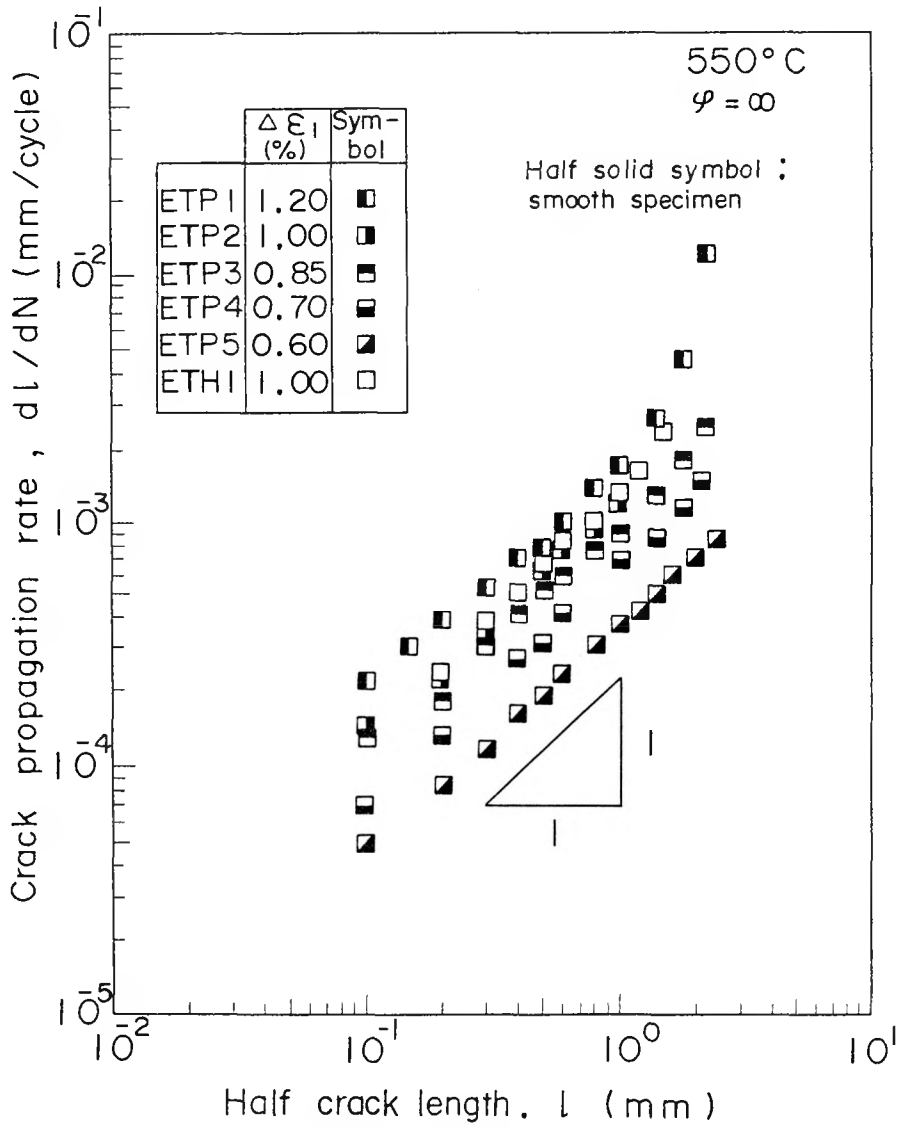

(b) $\varphi = \infty$

Fig. 5 (Cont.)

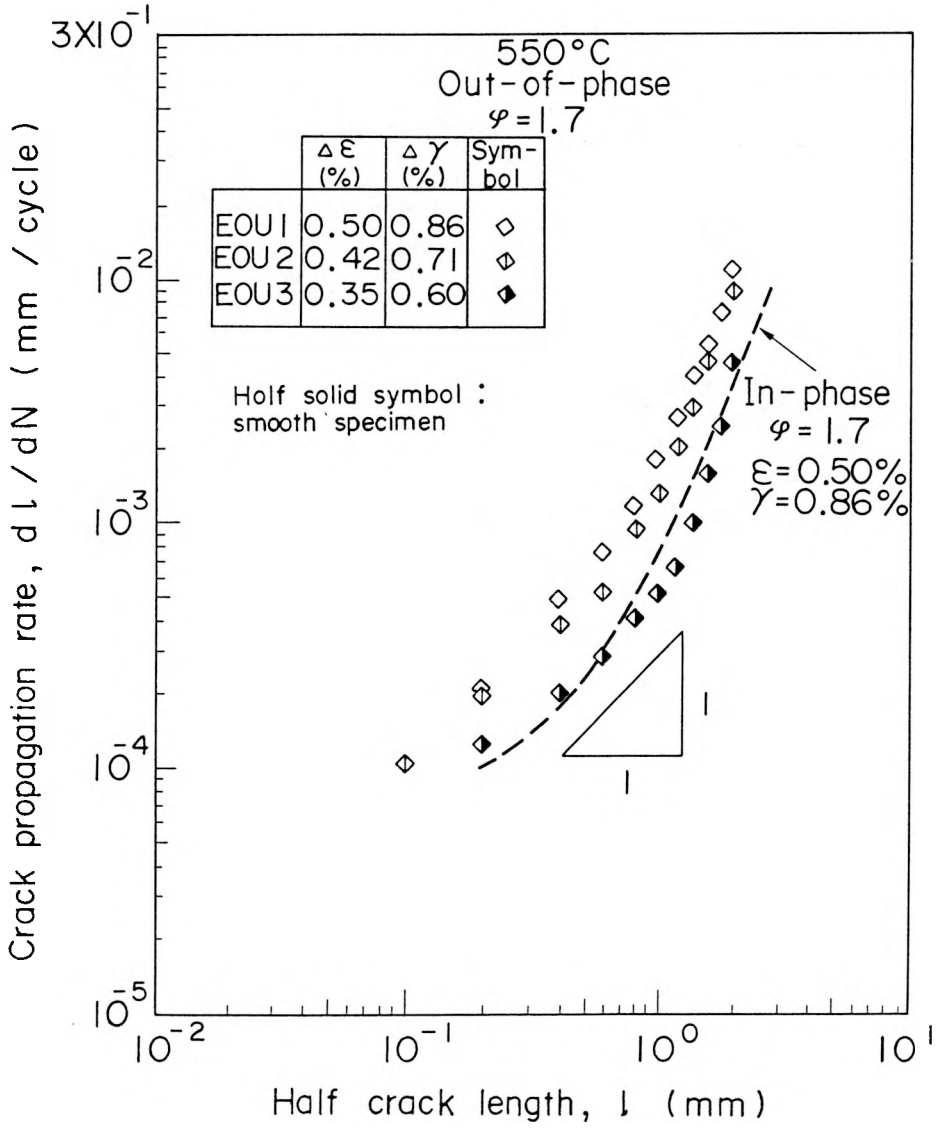

(c) φ = 1.7 (Out-of-phase)

Fig. 5 (Cont.)

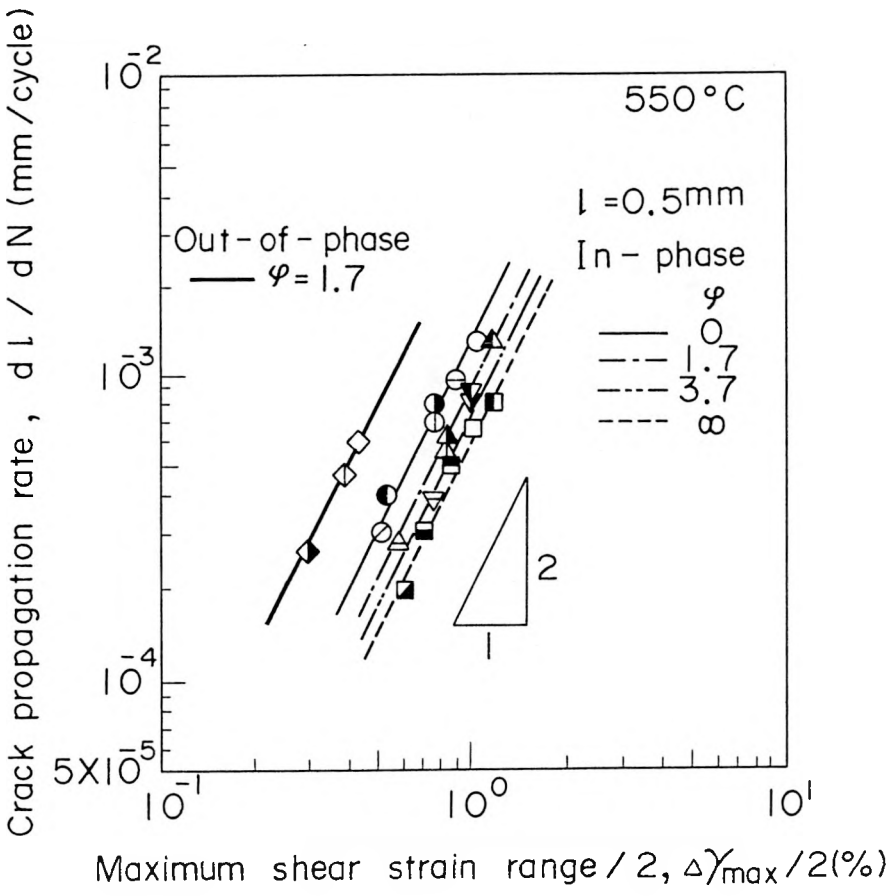
Crack propagation rate, dL / dN (mm/cycle)
10^{-2}
10^{-3}
10^{-4}
$5X10^{-5}$
10^{-1}
10^{0}
10^{1}
550°C
l =0.5mm
In-phase
φ
0
1.7
3.7
∞
Out-of-phase
φ= 1.7
2
1
Maximum shear strain range / 2, $\Delta\gamma_{max}/2$(%)

Fig. 6

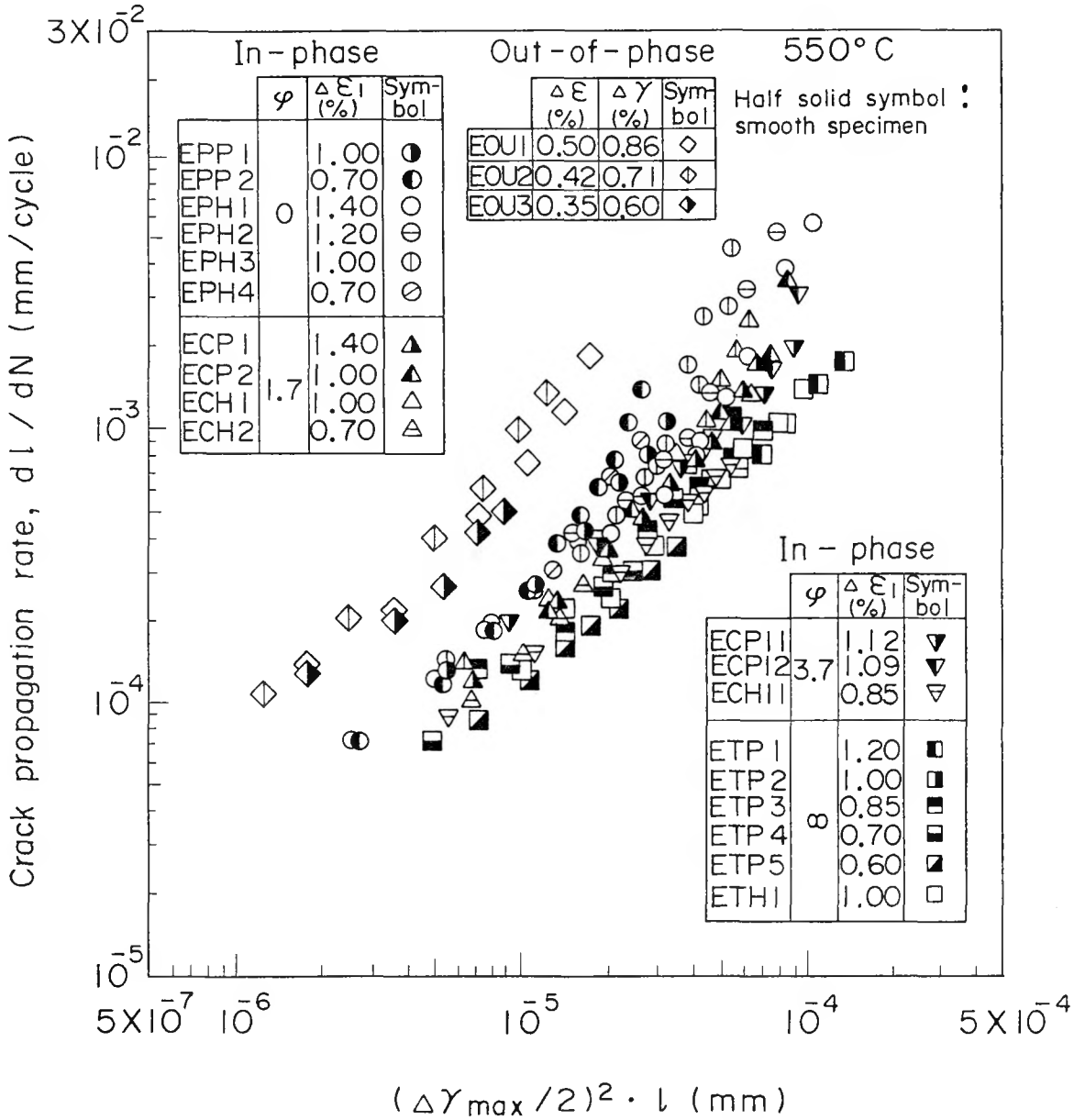

	φ	Δε1 (%)	Symbol
EPP1	0	1.00	
EPP2		0.70	
EPH1		1.40	
EPH2		1.20	
EPH3		1.00	
EPH4		0.70	
ECP1	1.7	1.40	
ECP2		1.00	
ECH1		1.00	
ECH2		0.70	

	Δε (%)	Δγ (%)	Symbol
EOU1	0.50	0.86	
EOU2	0.42	0.71	
EOU3	0.35	0.60	

	φ	Δε1 (%)	Symbol
ECP11	3.7	1.12	
ECP12		1.09	
ECH11		0.85	
ETP1	∞	1.20	
ETP2		1.00	
ETP3		0.85	
ETP4		0.70	
ETP5		0.60	
ETH1		1.00	

Fig. 7

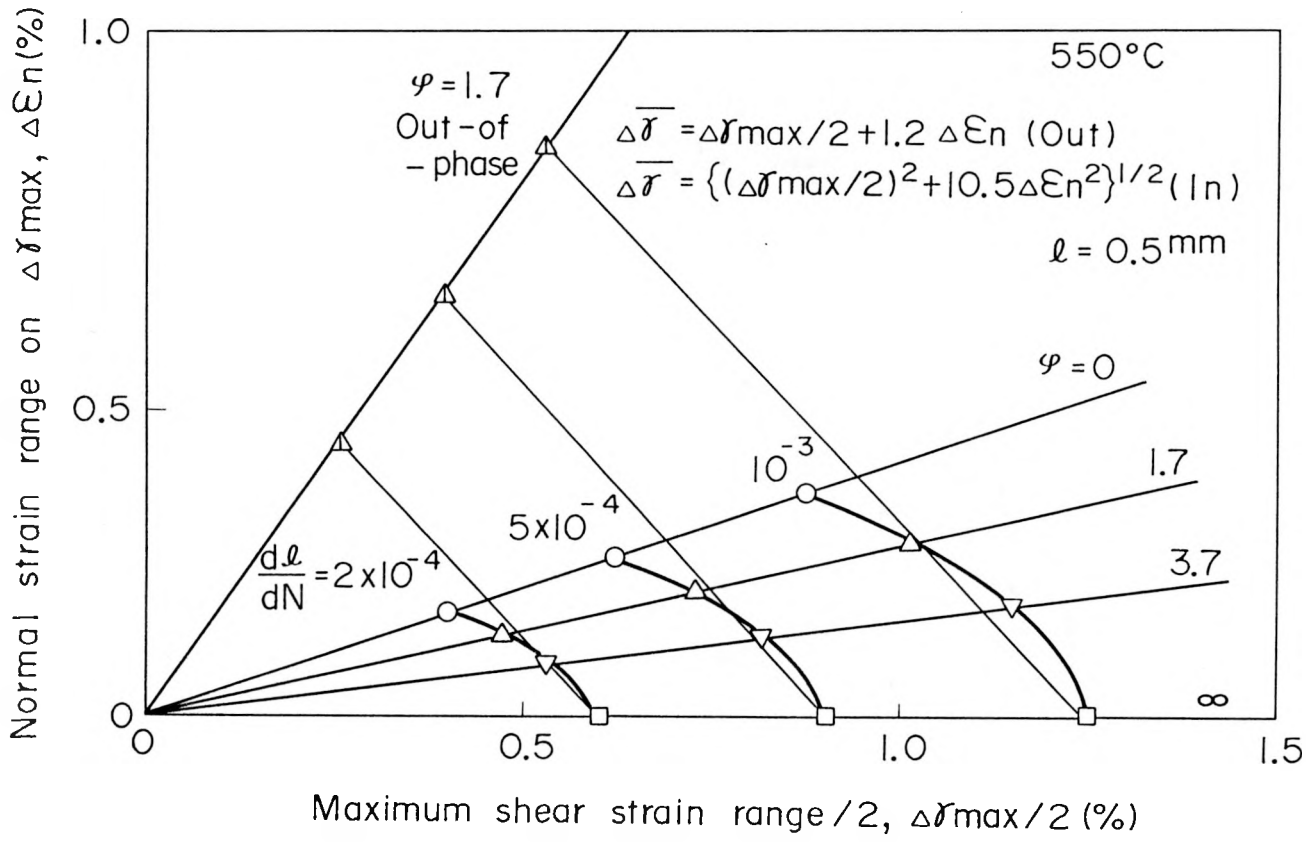
550°C
φ = 1.7
Out-of
– phase
Δγ̄ = Δγmax/2 + 1.2 ΔεN (Out)
Δγ̄ = {(Δγmax/2)² + 10.5Δεn²}^1/2 (In)
ℓ = 0.5 mm
φ = 0
1.7
3.7
∞
10^-3
5x10^-4
dℓ/dN = 2x10^-4
1.0
0.5
0
0
0.5
1.0
1.5
Normal strain range on Δγmax, ΔεN (%)
Maximum shear strain range/2, Δγmax/2 (%)

Fig. 8

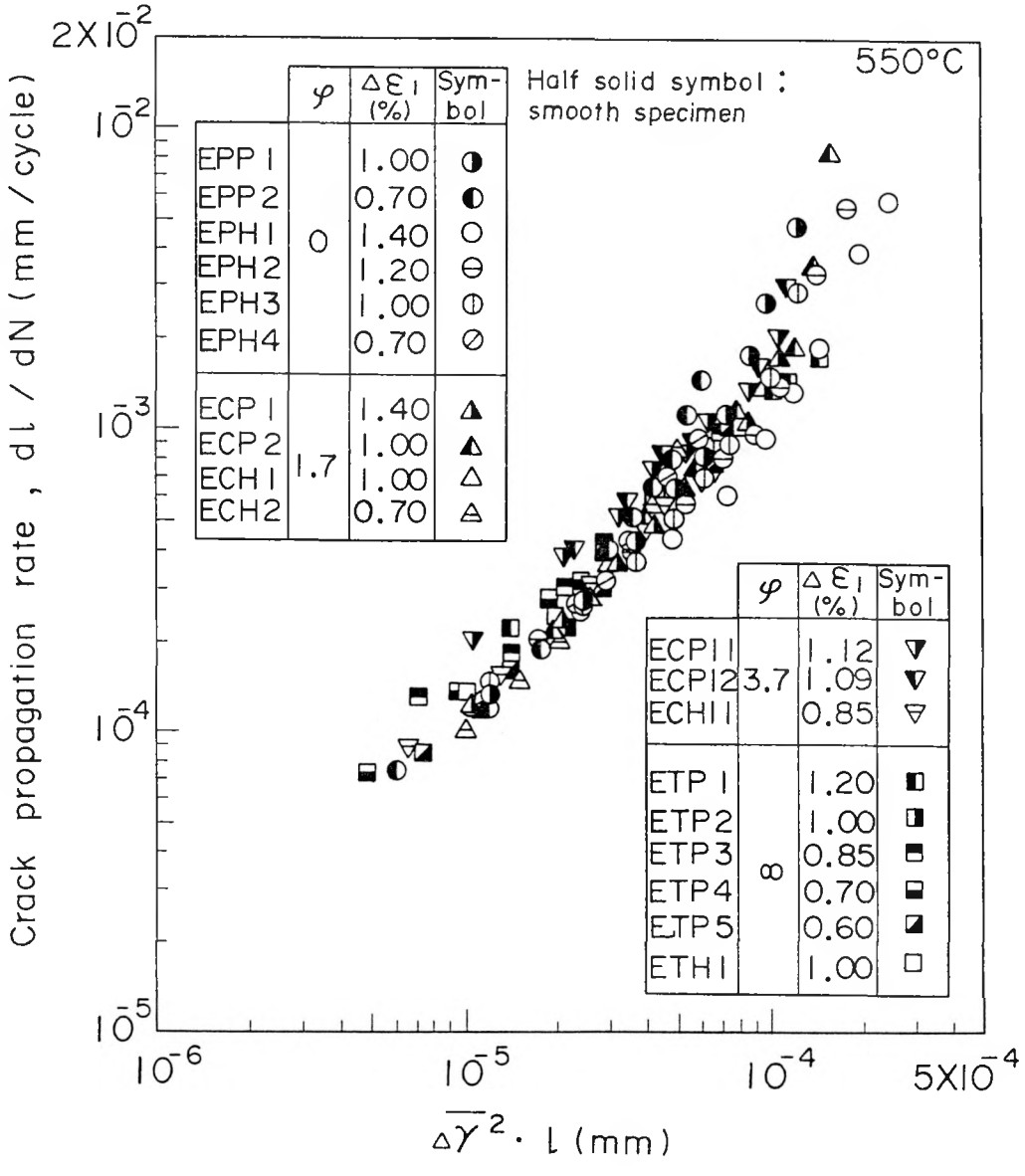
550°C
Half solid symbol : smooth specimen
Crack propagation rate , dl / dN (mm / cycle)
$\overline{\Delta\gamma^2} \cdot l$ (mm)
$2X10^{-2}$
10^{-2}
10^{-3}
10^{-4}
10^{-5}
10^{-6}
10^{-5}
10^{-4}
$5X10^{-4}$
φ | Δε1 (%) | Sym-bol
EPP1 | 0 | 1.00
EPP2 | 0 | 0.70
EPH1 | 0 | 1.40
EPH2 | 0 | 1.20
EPH3 | 0 | 1.00
EPH4 | 0 | 0.70
ECP1 | 1.7 | 1.40
ECP2 | 1.7 | 1.00
ECH1 | 1.7 | 1.00
ECH2 | 1.7 | 0.70
φ | Δε1 (%) | Sym-bol
ECP11 | 3.7 | 1.12
ECP12 | 3.7 | 1.09
ECH11 | 3.7 | 0.85
ETP1 | ∞ | 1.20
ETP2 | ∞ | 1.00
ETP3 | ∞ | 0.85
ETP4 | ∞ | 0.70
ETP5 | ∞ | 0.60
ETH1 | ∞ | 1.00

Fig. 9

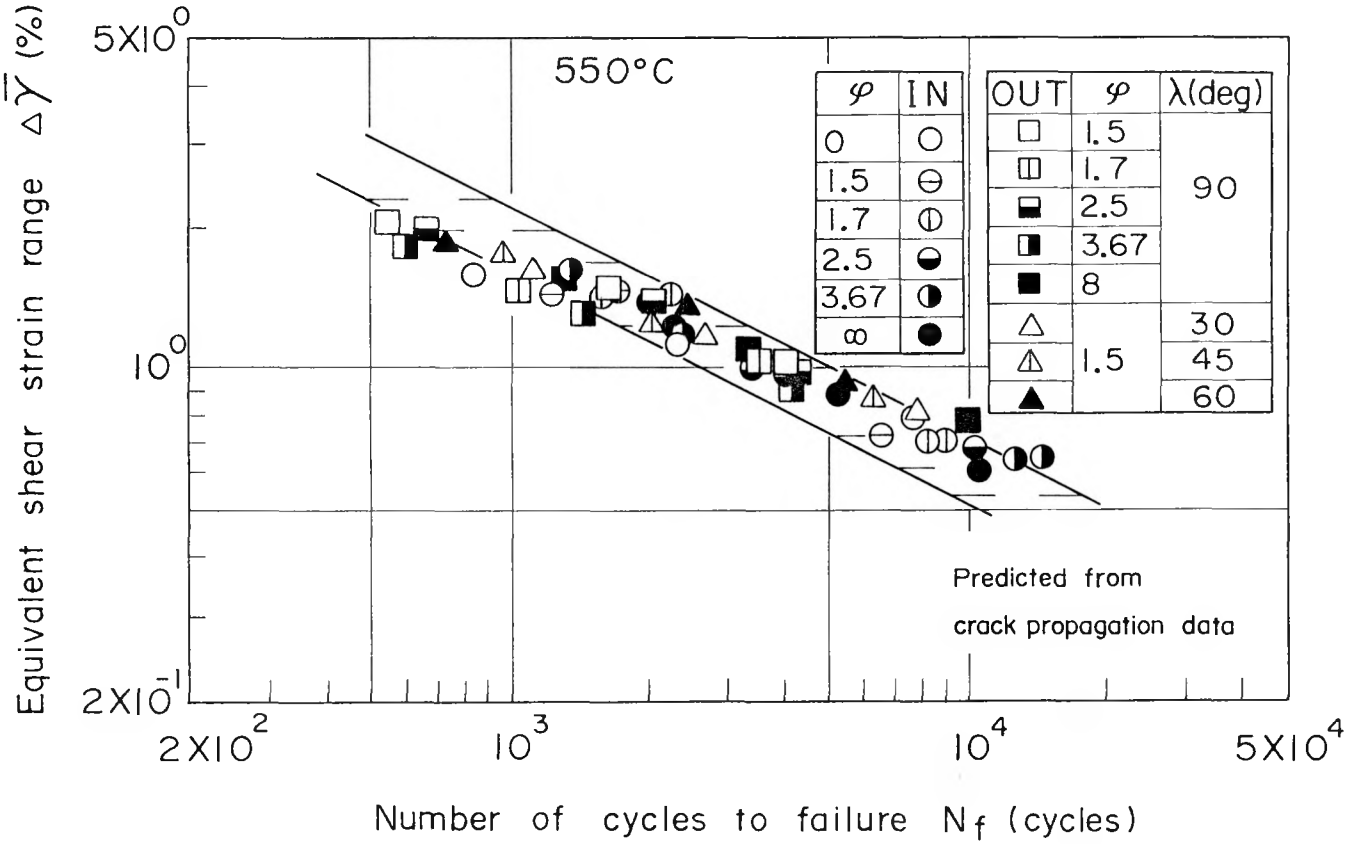
550°C
Equivalent shear strain range $\Delta\bar{\gamma}$ (%)
$5X10^0$
10^0
$2X10^{-1}$
$2X10^2$
10^3
10^4
$5X10^4$
Number of cycles to failure N_f (cycles)
φ | IN
0
1.5
1.7
2.5
3.67
∞
OUT | φ | λ(deg)
1.5
1.7
2.5
3.67
8
90
1.5
30
45
60
Predicted from
crack propagation data

Fig. 10